AIAA 2003–4261

MODEL-BASED COHERENT-STRUCTURE CONTROL OF TURBULENT SHEAR FLOWS USING LOW-DIMENSIONAL VORTEX MODELS

M. Pastoor, R. King
Measurement and Control Group,
Institute for Process and Plant Technology,
Technical University of Berlin, Berlin, GERMANY

B.R. Noack, A. Dillmann
Hermann-Föttinger-Institute of Fluid Mechanics,
Technical University of Berlin, Berlin, GERMANY

G. Tadmor
Department of Electrical and Computer Engineering,
Northeastern University, Boston, MA, U.S.A.

33rd AIAA Fluids Conference & Exhibit
June 23 – 26, 2003
Orlando, Florida

MODEL-BASED COHERENT-STRUCTURE CONTROL OF TURBULENT SHEAR FLOWS USING LOW-DIMENSIONAL VORTEX MODELS

Mark Pastoor*, Rudibert King†
Measurement and Control Group, Institute for Process and Plant Technology, Technical University of Berlin P2-1
Hardenbergstraße 36a, D-10623 Berlin, Germany

Bernd R. Noack‡, Andreas Dillmann§
Hermann-Föttinger-Institute of Fluid Mechanics, Technical University of Berlin HF1
Straße des 17. Juni 135, D-10623 Berlin, Germany

Gilead Tadmor¶
Department of Electrical and Computer Engineering, Northeastern University
440 Dana Research Building, Boston, MA 02115, U.S.A.

Abstract

In this study, a flow control strategy is presented for manipulating coherent shear-flow structures. As a benchmark problem, the transitional flow around a backward-facing step with local acoustic actuation at the upper edge is chosen. The strategy is based on a hierarchy of low-dimensional vortex models and targets the use of control-theory methods for control design. The hierarchy ranges from an one-vortex model which describes the vortex roll-up and shedding to a vortex-blob model which resolves the formation of Kelvin-Helmholtz vortices and the dynamics of the recirculation zone with a few hundred vortices. The higher-dimensional variants predict well the frequency-dependent reduction of the recirculation zone with harmonic actuation. The Lagrangian vortex models incorporate a continuous production, merging, and annihilation of vortices, but this hybrid nature excludes the use of many control-theory methods. Hence, one- and two-dimensional Eulerian vortex models employing a remeshing technique are proposed. The dynamics of these Eulerian variants define a continuous evolution in a phase space with fixed dimension and are hence better suited for control-theory and dynamics-systems approaches.

*Research engineer. Corresponding author: phone: ++49-30-314.79574, x24100; fax: x21129; e-mail: mark.pastoor@tu-berlin.de
†Professor
‡Research engineer
§Professor
¶Associate Professor

I Introduction

The current study is part of the efforts at the Collaborative Research Center (Sfb 557) "Control of Complex Turbulent Shear Flows" at the Technical University Berlin. The goal is modeling and controlling coherent shear-flow structures using low-dimensional coherent-structure models and control-theory methods. The target is to develop flow control strategies leading to robust online-capable model-based controllers in benchmark experiments.

The model-based control is based on a hierarchy of flow models ranging from accurate direct numerical simulations (DNS) to empirical black-box models (see Fig. 1). At an intermediate ('grey box') level of this hierarchy, the coherent structures are described by low-dimensional Galerkin and vortex methods, following studies of Ghoniem and coworkers.[1,2] Thus, a compromise is realized between the need of sufficiently low-dimensional models for the application of control-theory methods and the

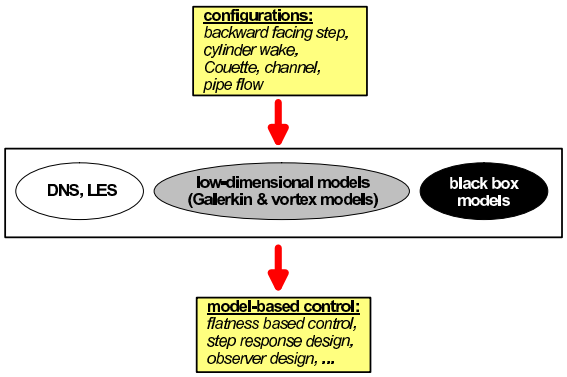

Figure 1: *Principal sketch of the hierarchy of model-based control strategies*

need of sufficiently high-dimensional flow representations for an acceptable accuracy.

The control strategy is developed for the actuated flow around the backward-facing step as a well investigated benchmark problem,[3] particularly for combustion related problems.[4,5] The experimental setup[3] and the associated coherent flow structures[6] are shown in Fig. 2. The flow structures are

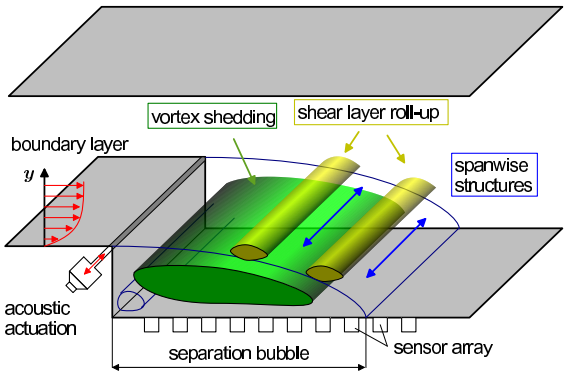

Figure 2: *Principal sketch of the experimental setup and the dominating structures of the flow around the backward-facing step: vortex-shedding, shear-layer roll-up, and spanwise structures.*

monitored using arrays of microphones at the bottom wall.[7] The effect of the shear-layer mixing is indicated by the size of the separation bubble, or, equivalently, by the reattachment length. Numerical and experimental data yield a reattachment length of 6.5 step heights for the chosen configuration at a Reynolds number of $Re_h = 4000$ [Garwon, private communication 2002]. The reattachment length x_R is defined by the time-averaged length of the separation bubble indicated by vanishing wall stress.

The actuation of the flow is carried out with zero-net flux pressure disturbances produced with a slot-loudspeaker at the edge of the step. The control problem is to prescribe a given reattachment length with an energy-efficient actuation in dependency of the pressure signals.

The flow around the step is characterized by three dominating structures:

(A) a vortex-shedding process,

(B) the roll-up of the separating boundary-layer into Kelvin-Helmholtz-type shear-layer vortices, and

(C) the spatial evolution of spanwise structures.

These structures are schematically shown in Fig. 2 and can be inferred from a simulation snapshot in Fig. 3.

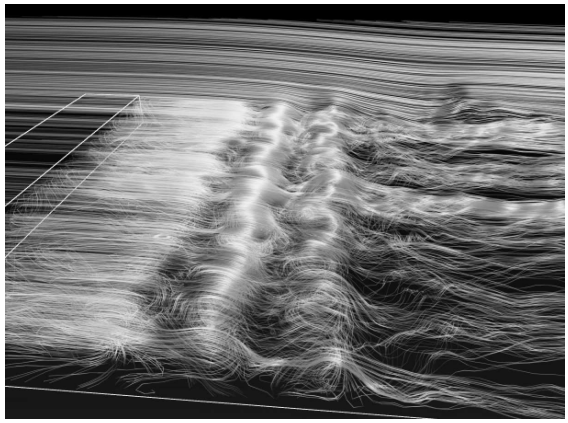

Figure 3: *Streamlines of a numerical solution of H.-J. Kaltenbach[8] at $Re_h = 3000$ illustrating the structures in Fig. 2. The visualization technique is described by Weinkauf et al.[6]*

The dominant coherent structures found in experiments and simulations are a crucial prerequisite for the development of low-dimensional modeling approaches. Two approaches are pursued, Galerkin and vortex models. Results of the Galerkin ansatz have been described elsewhere.[9] In this paper, an effort to develop vortex models is outlined for the two-dimensional coherent structures (processes A and B). Process C may be described by a three-dimensional vortex-filament model for the initial part of the shear-layer.[10]

In the following section (II), the constitutive elements of the vortex methods are described. In Sec. III, the results for the natural and actuated flow are outlined. A discussion of system reduction and actuation aspects is presented in Sec. IV. The main results are summarized in Sec. V with an outlook.

II Hierarchy of vortex models

In this section, a hierarchy of vortex models is described. First (Sec. II.1), an overview of the hierarchy and its constitutive elements is given. These elements are detailed in Secs. II.2–II.10.

II.1 Outline

On a kinematic level, all presented low-dimensional models approximate the vorticity distribution by adding vortices to the two-dimensional potential flow. The dynamics are derived from potential theory using Biot-Savart's law for the induced velocity and Helmholtz's laws for preservation of circulation.

The current study generalizes a vortex model of the actuated diffuser flow[11] by more physical assumptions obtained from Navier-Stokes simulations and by the development of an Eulerian counterpart with a constant number of vortices. Figure 4 displays the model hierarchy. The Lagrangian variant (Fig. 4*a*) is based on the continuous production of vortices. The vortices are later merged with other vortices. The circulation is reduced near the wall and far downstream the vortices are annihilated. In the one-dimensional Eulerian vortex-slice model (Fig. 4*b*), the vorticity of a transverse slice is lumped to a single vortex which has the circulation of the whole slice. The vortex slides on a vertical line in the middle and assumes the transverse position of the vorticity center. Similarly, the two-dimensional Eulerian vortex model (Fig. 4*c*) lumps the vorticity in the center of each area element of a given mesh. Vorticity transport of the Eulerian variants is described by a remeshing technique (see Sec. II.10). A three-dimensional Navier-Stokes simulation (Fig. 4*d*) is employed for model development and validation.

The main elements of the vortex models are visualized in Fig. 5 and detailed in the following sections. The no-penetration boundary condition at the wall is enforced using a conformal mapping from the upper half-plane onto the backward-facing step with the upper wall (see Sec. II.2). The boundary condition is easily enforced in the computational domain. Thus, the potential solution (see Sec. II.3) is represented by a single source in the computational domain. Acoustic actuation is mimicked by a harmonic sink-source (see Sec. II.4). The Oseen vortex and its mirror image transforms into a vortex solution in the physical domain which respects the no-penetration condition at the wall (see Sec. II.6). The motion of this vortex is determined by the potential solution, the actuation field and the induced velocity from Biot-Savart's law (see Sec. II.5). The vortex

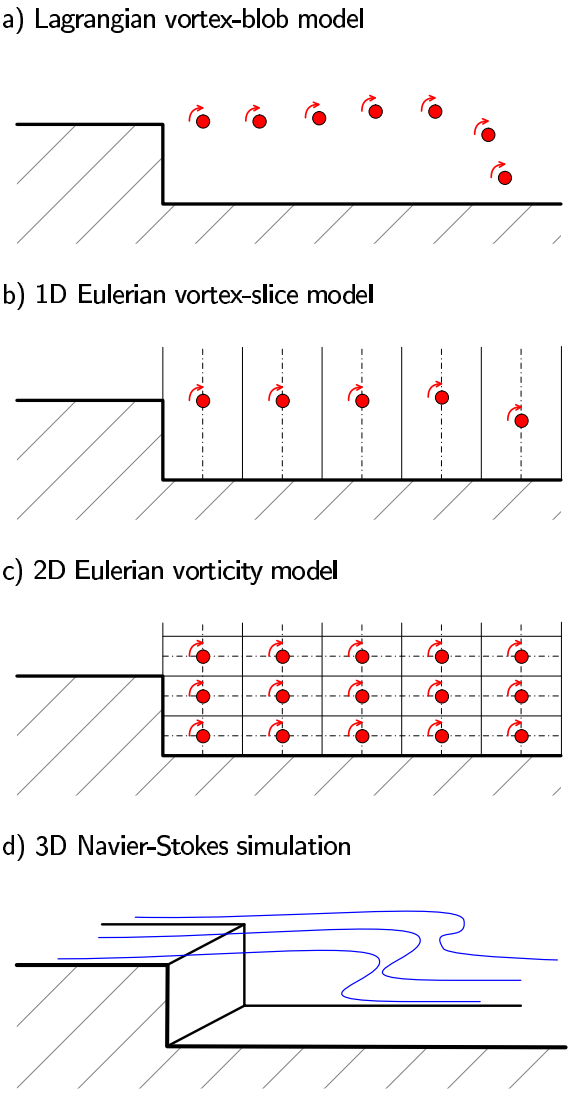

Figure 4: *Outline of the model hierarchy. The hierarchy includes (a) a Lagrangian vortex-blob model, (b) a one-dimensional Eulerian vortex-slice model, (c) a two-dimensional Eulerian vortex model, and (d) a Navier-Stokes simulation. The vortices are indicated by solid circles. The side constraints on the vortex positions of the Eulerian models are visualized by dashed lines. Each vortex of the Eulerian models lumps the vorticity on the corresponding rectangular region which is indicated by solid lines.*

production at the step follows a generalized Kutta condition[12] which is validated against the simulation (see Sec. II.7). The vorticity is annihilated near the wall and the decay-rate is estimated from simulation (see Sec. II.8). Similar modeling assumptions are used in Lagrangian and Eulerian approaches. A distinguishing feature of the Lagrangian models is a merging mechanism in which the number of vor-

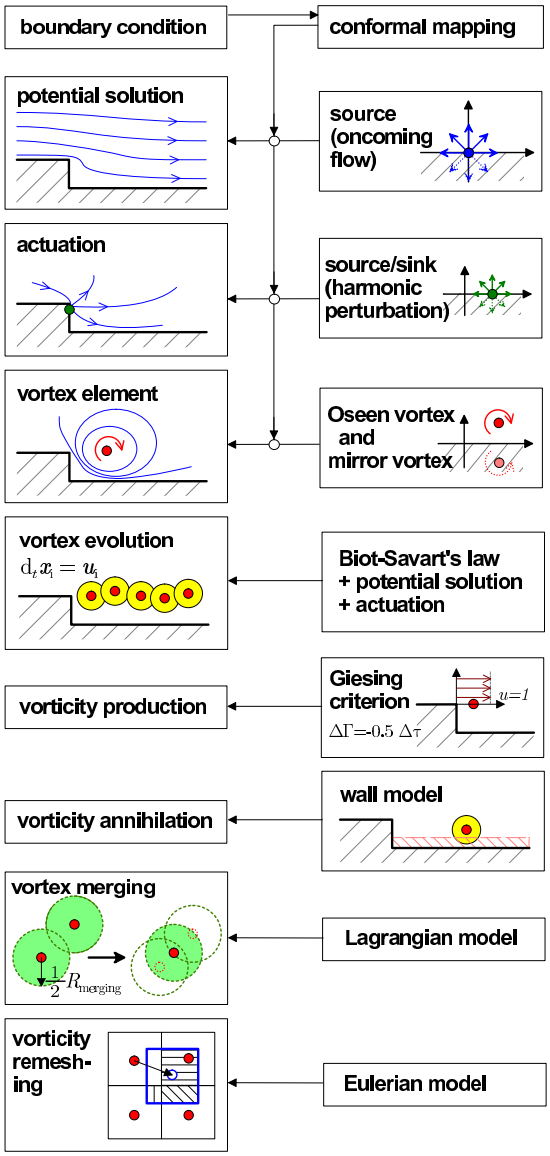

Figure 5: *Elements of the vortex models. These elements include models for boundary conditions (see Sec. II.2), potential flow (see Sec. II.3), actuation (see Sec. II.3), vortex element (see Sec. II.6), vortex dynamics (see Sec. II.5), vorticity production (see Sec. II.7), vorticity annihilation (see Sec. II.8), vortex merging (see Sec. II.9) and vorticity remeshing (see Sec. II.10).*

tices is reduced further downstream (see Sec. II.9). A distinguishing feature of the Eulerian model is a transport of vorticity between neighboring vortices by a remeshing technique[13] (see Sec. II.10).

II.2 Conformal mapping

At the upper and lower walls, the no-penetration condition is imposed. Following Coller *et al.*[11] and Cortelezzi *et al.*,[14] this condition is computationally more easily satisfied employing a conformal map as compared to a computational panel approach.[15] This map bijectively transforms the computational domain, the upper half-plane, into the physical domain. In the computational domain, the no-penetration condition with discrete vortices is satisfied by introducing mirror vortices (see Sec. II.6) with the abscissae as the axis of reflection.

The conformal mapping from the computational domain, $\zeta = \xi + \imath\eta$, into the physical domain, $z = x + \imath y$, is visualized in Fig. 6. This mapping is

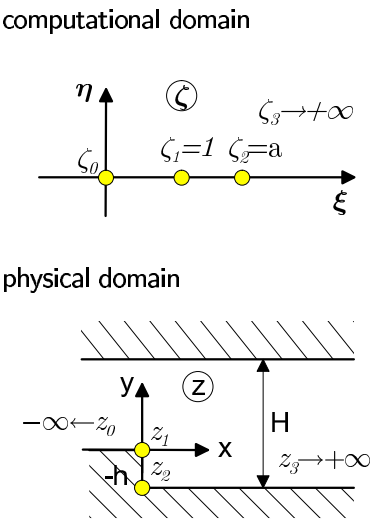

Figure 6: *Schwarz-Christoffel transformation of the backward-facing step from the computational into the physical domain. This transformation maps $\zeta_1 = 1$ on the upper edge of the step ($z_1 = 0$) and $\zeta_2 = a$ on the lower edge ($z_2 = -\imath h$). The negative abscissae corresponds to the upper wall, and the positive abscissae to the lower wall. Therefore, the origin of the ζ-plane is mapped on $z_0 \to -\infty$.*

described by a Schwarz-Christoffel transformation

$$\frac{\mathrm{d}z}{\mathrm{d}\zeta} = C_1 \frac{1}{\zeta}\sqrt{\frac{\zeta - 1}{\zeta - a}}, \qquad z, \zeta \epsilon \mathbb{C}. \qquad (1)$$

The map $z(\zeta)$ is obtained by an analytical integration of Eq. (1), yielding

$$z(\zeta) = C_1 \left(\frac{1}{\sqrt{a}} \ln \frac{\sqrt{a}t(\zeta) - 1}{\sqrt{a}t(\zeta) + 1} - \ln \frac{t(\zeta) - 1}{t(\zeta) + 1} \right) + C_2,$$

$$\text{where} \quad t(\zeta) = \sqrt{\frac{\zeta - 1}{\zeta - a}}.$$

The constants $a = H/(H-h)$, $C_1 = H/\pi$ and the integration constant $C_2 = -\imath h$ are obtained from the equation of continuity and from geometrical considerations. The inverse mapping $\zeta(z)$ is calculated numerically with the Newton method. No analytical solution has been found.

II.3 Potential flow

The vortex models yield potential flow solutions of the Navier-Stokes equation with singularities at the vortex positions. The conformal mapping is used to satisfy the no-penetration condition at the walls in an efficient manner. The vorticity-free potential flow solution is generated by a point source at the origin of the computational domain ($\zeta_0 = 0$, see Fig. 6). The source strength Q corresponds to the flow rate in each cross section of the physical domain. This induces a complex velocity, that can be calculated from the source's potential $W_s^\zeta(\zeta)$,

$$\begin{aligned} w_s^\zeta(\zeta) = \frac{\mathrm{d}W_s^\zeta(\zeta)}{\mathrm{d}\zeta} &= \frac{Q}{2\pi}\frac{1}{\zeta-\zeta_0} \\ \text{with} \quad Q &= 2\,u_\infty\,(H-h), \end{aligned}$$

where u_∞ denotes the velocity of the oncoming flow. The velocity field of this source in the physical domain describes a potential flow around the step without separation. The abscissae of the ζ-plane represents the wall stream-lines in the physical domain.

The superposition principle of potential flow theory allows to compute the complex velocity in the computational domain by a superposition of sinks, sources and point vortices. The transformation into the physical domain is obtained by applying the chain rule. The corresponding velocities in the physical domain are

$$u - \imath v = w = \frac{\mathrm{d}W^z}{\mathrm{d}z} = \frac{\mathrm{d}W^\zeta}{\mathrm{d}\zeta}\frac{\mathrm{d}\zeta}{\mathrm{d}z}.$$

II.4 Actuation

The actuation is modeled by a harmonic oscillating source near the trailing edge of the step — following the authors work for a similar diffuser configuration.[11] The corresponding velocity field reads

$$w_a^\zeta(\zeta,t) = \left.\frac{\partial W_a^\zeta(\zeta,t)}{\partial\zeta}\right|_t = \frac{Q_a(t)}{2\pi}\frac{1}{\zeta-\zeta_a}.$$

Here, the position ζ_a is located at the center of the actuator exit. Its strength $Q_a(t)$ depends on the selected actuation. The instantaneous mass flux into the upper half-plane is chosen to be similar to the corresponding quantity of the acoustic actuator in experiment.

A more refined actuation model consists of a representation of the jet from the actuator slot by a vorticity discretization of the shear-layers. The Lagrangian model employs the point-source model in order to keep the number of vortices computationally manageable. The 2D Eulerian model employs the refined actuation representation in a coarse resolution dictated by the chosen grid.

II.5 Vortex dynamics

The no-penetration condition for potential flow with a vortex is fulfilled with a (virtual) mirrored vortex with mirrored coordinates and opposite circulation. Analogously, an ensemble of vortices is supplemented by their mirror vortices. Thus, vanishing global vorticity is preserved. The induced complex velocity of a vortex is given by the derivative of its complex potential $W_v^\zeta(\zeta)$. The $N_v(t)$ vortices at the time t in the physical domain induce the complex velocity

$$\begin{aligned} w_v^\zeta(\zeta) &= \frac{\mathrm{d}W_v^\zeta(\zeta)}{\mathrm{d}\zeta} \\ &= \sum_{i=1}^{N_v(t)} \frac{\imath\Gamma_i}{2\pi}\left(\frac{1}{\zeta-\overline{\zeta_{v,i}}} - \frac{1}{\zeta-\zeta_{v,i}}\right), \end{aligned}$$

where $\zeta_{v,i}$ denotes the current position of the i-th vortex and Γ_i its circulation. The overbar indicates the complex conjugate of a complex number. The circulation Γ_i of each vortex is preserved according to Kelvin's law.

Thus, the velocity of i-th vortex in the physical domain is expressed by the sum of potential flow, the actuation field, and the vortex-induced field $w_v^{\zeta\star}$ discounting self-induction,

$$u_i - \imath v_i = \left[w_s^\zeta + w_a^\zeta + w_v^{\zeta\star}\right]\left.\frac{\mathrm{d}\zeta}{\mathrm{d}z}\right|_{z_{v,i}}.$$

The only difference between $w_v^{\zeta\star}$ and w_v^ζ is the singularity at the vortex position.

II.6 Vortex element

Up to now, a point vortex discretization has been assumed in agreement with potential flow theory. The discontinuity in the vortex field is removed in a more refined model by *Hamel* and *Oseen*. Their solution for the azimuthal velocity u_φ smoothly connects a Rankine vortex core at $r \to 0$ with the potential vortex at $r \to \infty$,

$$u_\varphi(r) = \frac{\Gamma(r)}{2\pi\, r}, \tag{2}$$

where $\Gamma(r) = \Gamma_0 \left(1 - e^{-\frac{r^2}{4\kappa}}\right)$. The parameter κ determines the equivalent Rankine core radius $2\sqrt{\kappa}$. The Hamel-Oseen solution of the Navier-Stokes equation is described by Eq. (2) and $\kappa(t) = \nu t$ with the kinematic viscosity ν. The initial core radius at the step is chosen to be similar to the boundary-layer thickness like in similar vortex models.[16] The temporal growth is implemented in the Lagrangian variant but has little effect at the considered Reynolds number of $Re_h = 4000$.

II.7 Vorticity production at the edge

Experiments and simulations (see Fig. 3) indicate a straight shear-layer emerging from the edge of the step in the direction of the oncoming flow. Giesing[12] proposes a *generalized Kutta condition* for the idealized infinitely thin shear-layer in an inviscid flow. According to this condition, the shear-layer is aligned with the oncoming flow and associated with the vorticity production rate

$$\frac{d\Gamma}{dt} = -\frac{1}{2} u_\infty^2.$$

This criterion is in good agreement with experiment and simulation.

In the vortex models, the Giesing solution is discretized by inserting a vortex with the convective velocity $u_c = u_\infty/2$ and circulation $\Gamma_0 = -1/2\, u_\infty^2 \Delta t$ at $x_{v,0} = u_c\, \Delta t$ and $y_{v,0} = 0$ at discrete time steps Δt. To avoid numerical problems with the potential flow singularity at the upper edge, the vortices are lead a short distance away from the singularity.

II.8 Vorticity annihilation at the wall

In streamwise direction, the flow forgets about stumbling over the step and approaches a channel flow with a small boundary-layer. This boundary-layer is due to the no-slip condition and effectively absorbs the vorticity. Vortex models are based on the Euler equation with its associated no penetration condition, i.e. cannot incorporate effects of the boundary-layer. Hence, vorticity is annihilated near the wall. A reasonable agreement between the vorticity distribution of vortex models and simulation is obtained with

$$\frac{d}{dt}\Gamma = -\Gamma,$$

whenever the vortex radius (equivalent Rankine core) touches the wall.

II.9 Vortex merging in Lagrangian models

A degree of freedom of our model is the number of vortices consistent with the required low-dimensionality. The perpetual creation of new vortices increases the order of our model. The dimension can be reduced by merging two vortices when their distance is below a critical value.

The result of a merging process is one vortex with the combined circulation located at the barycentre of both predecessors. The choice of the critical merging radius has strong influence on the dimension of the model, but has small effect on the coherent structure if the merging radius is not too large. A reasonable compromise between accuracy and dimensionality is obtained by a merging distance which increases linearly in streamwise direction from zero after five step heights ($x = 5$). Thus, the initial shear-layer is not perturbed by the merging process.

II.10 Remeshing in Eulerian models

In the Eulerian models, the vortex positions are constrained. Vortex transport is considered by a simple remeshing technique.[13] In the 2D model, the rectangle associated with the vortex is advected during the integration time step with the velocity of its center. After the time step, part of the circulation of the vortex is distributed to its neighbors in proportion to the overlapping regions (see Fig. 4) The total circulation is preserved. In the 1D model an analogous model is used.

III Results

In this section, the natural and actuated flow is discussed for the Navier-Stokes simulation (Sec. III.1), for the Lagrangian vortex model (Sec. III.2), and the Eulerian counterpart (Sec. III.3).

III.1 Navier-Stokes simulation

The incompressible flow around a backward-facing step is simulated by a large-eddy simulation. The incoming boundary-layer is steady and laminar and has a thickness which is about one tenth of the step height. The simulation data has been kindly provided by Maiko Garwon. The domain and the boundary condition are similar to simulations of Kaltenbach *et al.*[8] including the spanwise periodicity of 6 step heights.

Figure 7 shows snapshots in a computational subdomain for the natural and actuated flow. The snapshots are averaged in spanwise direction. Evidently, the actuation enhances the vortex formation in the initially laminar shear-layer and reduces significantly the recirculation length. This length is monitored during a post-transient part of the simula-

tion which contains 150 convective time units without actuation followed by 150 units with actuation (Fig. 7*c*). The transition process before the reattachment line can be inferred from the spottiness of the vorticity.

a) Natural flow

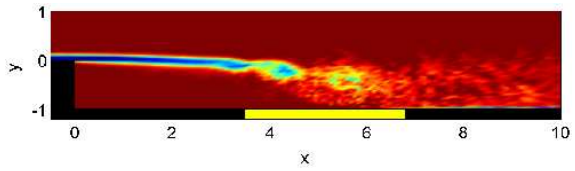

b) Actuated flow at $St_h = 0.45$

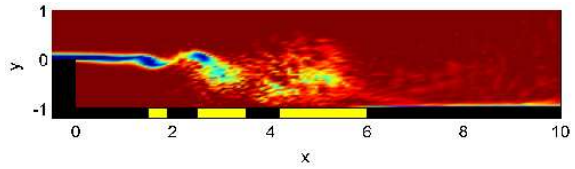

c) Recirculation length in dependency of the time

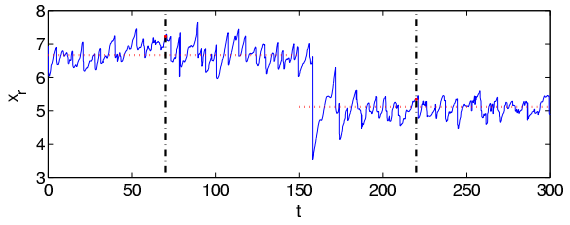

Figure 7: *Actuation effect predicted by the Navier-Stokes simulation. The top (middle) figure displays the vorticity distribution under natural (actuated) conditions. In these flow visualizations, the recirculation region with negative wall-stress is indicated by a grey bar on the lower wall. In the bottom figure, the recirculation length x_R is monitored for the period $t = 0 - 300$. Actuation starts at $t = 150$. The instances of the displayed snapshots are indicated by horizontal dashed lines.*

It should be noted that the actuated flow displays several regions of reverse flow. The reattachment length is defined as the first zero of the wall-stress downstream of the global minimum of this quantity.

III.2 Lagrangian vortex model

Figure 8 displays snapshots of the natural and actuated flow computed by the Lagrangian vortex model. The laminar shear-layer is discretized by a continuous chain of vortices which roll-up into Kelvin-Helmholtz-type vortices. The natural shedding frequency is about $St_h = 0.4$ and in good agreement with the simulation. The reattachment length is under-predicted by 10% which can be considered as small for a low-dimensional model. Also the effect of actuation is well represented in several aspects. These aspects include a more rapid vortex roll-up, pronounced vortex pairing, several regions of reverse flow and a reduced recirculation length.

a) Natural flow

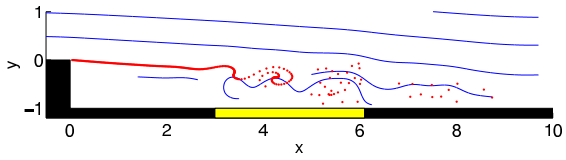

b) Actuated flow at $St_h = 0.4$

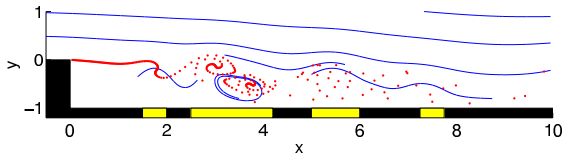

c) Recirculation length in dependency of the time

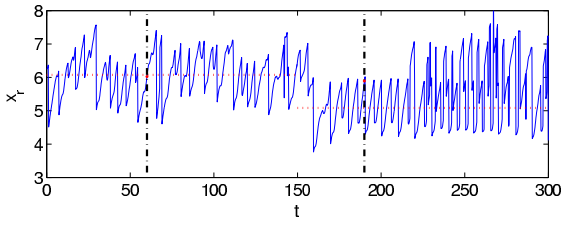

Figure 8: *Same as Fig. 7, but for the Lagrangian vortex model. Here, the flow is visualized with streamlines and the vortex positions as solid circles. The negative wall-stress regions correspond here to regions of reverse flow.*

The inviscid vortex models are approximations of the Euler solutions and the wall velocity plays the same role as the wall stress in the corresponding Navier-Stokes solutions. This analogy extends to the definition of the reattachment length as the first zero of the tangential flow velocity downstream of its global minimum.

III.3 Eulerian vortex model

Figure 9 displays snapshots of the natural and actuated flow computed by the Eulerian vortex model. This model exhibits smooth laminar representatives of the coherent structures in the simulation and reproduces the actuation effect.

a) Natural flow

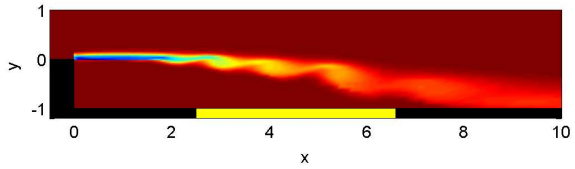

b) Actuated flow at $St_h = 0.4$

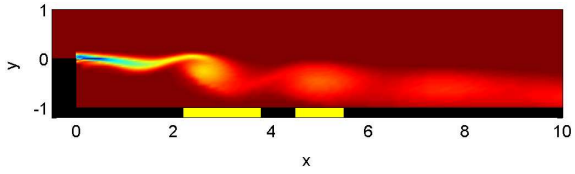

c) Recirculation length in dependency of the time

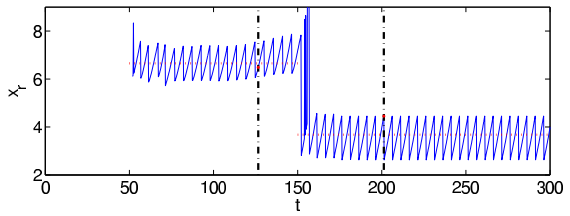

Figure 9: *Same as Fig. 7, but for the Eulerian vortex model.*

The figure incorporates the whole two-dimensional remeshing grid. This grid accommodates 100×30 vortices. The number of grid elements is much smaller than the $256 \times 80 \times 64$ volume elements used in the large-eddy simulation. It should be noted that the computational domain of the Eulerian model is two-dimensional and contains only 6.6% of the longitudinal section of the corresponding three-dimensional domain. This difference elucidates a well-known advantage of vortex models for confined vorticity distributions in the treatment of boundary conditions.[17]

This Eulerian model requires about 10 times more vortices than the Lagrangian variant of Sec. III.2. Yet, the computational loads per convective time unit are comparable, since the velocity at each vortex is a linear functional of the circulations and the actuation amplitude with a pre-determined matrix.

IV Discussion

In this section, the sensitivity of the vortex models with respect to physical and model parameters is discussed. In particular, the possibility of a system reduction is described for the Lagrangian and Eulerian models in Secs. IV.1 and IV.2, respectively. Open- and closed-loop characteristics are outlined in Sec. IV.3.

IV.1 System reduction of Lagrangian models

The merging radius plays an important role for the Lagrangian models. In particular, a continuous hierarchy is exemplified in Fig. 10 for natural flow. If the merging radius is several step heights, all vortices are immediately absorbed by a growing single vortex (see Fig. 10*a*). This vortex moves away from the lower corner with increasing circulation until it is swept away by the free stream. Thus, the dead-water zone and the vortex shedding is qualitatively mimicked by this 'least-order' model. However, the least-order representation cannot resolve the actuation effect, since this effect is based on the shear-layer dynamics. This dynamics has to be resolved by a chain of vortices — at minimum a several dozens in the near-field. This is achieved by decreasing the merging radius below the equivalent Rankine core. The

a) 'Least-order' model (1 vortex)

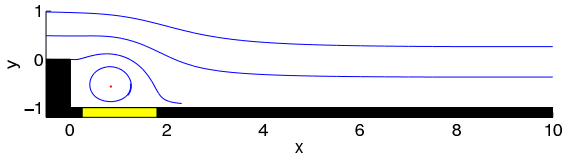

b) Low-order model (<100 vortices)

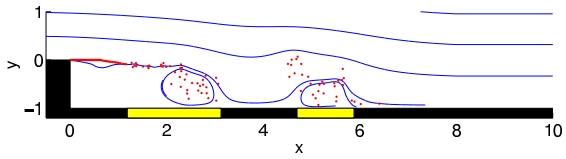

c) Higher-order model (~300 vortices)

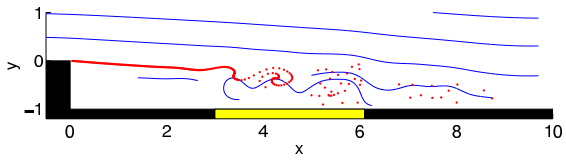

Figure 10: *Hierarchy of Lagrangian vortex models in dependency of the merging radius. Representative snapshots are shown for a 'least-order,' a low-order, and a higher-order model from top to bottom. The only difference between these models is the merging radius which decreases from top to bottom. The flow is visualized as in Fig. 8.*

observed initial steady shear-layer formation requires a sufficient density of these vortices. An increased steady region can be seen from the snapshots of the low-order (Fig. 10*b*) and the higher-order model (Fig. 10*c*). If the chain of vortices 'breaks' too early, this adds non-physical noise and promotes an earlier shear-layer roll-up.

IV.2 System reduction of Eulerian models

On the one hand, simulations of Eulerian model with different meshes indicate that the mesh should not be much coarser than the LES grid. Otherwise the shear-layer instability and the actuation effect cannot be reasonably resolved. On the other hand, about 50% of the vortices of the reference grid in Sec. III.3 do not participate in the vorticity transport and can be neglected. In addition, a further reduction of the vortex number is possible by lumping grid cells in downstream direction — in analogy to the Lagrangian vortex merging.

IV.3 Actuation effect and controller design

The vortex models predict well the optimal actuation frequency for time-harmonic open-loop control. This behavior is exemplified for the Lagrangian models in Fig. 11.

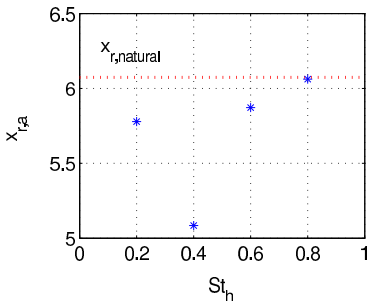

Figure 11: *Actuation prediction of Lagrangian vortex models in dependency of the Strouhal frequency. The symbols show some averaged recirculation lengths x_r in dependency of the actuation Strouhal frequencies St_h.*

The mathematical form of Eulerian models allows the use of control-theory methods in contrast to the hybrid Lagrangian models. Figure 12 outlines how the one- and two-dimensional Eulerian approach can be employed for validation purposes besides observer and closed-loop controller design.

It may be noted that the one-dimensional Eulerian model did not encourage its use as a coherent-structure representation, but was very useful for validation purposes. For instance, the vorticity annihilation has been calibrated against the simulation with the one-dimensional shear-layer approximation.

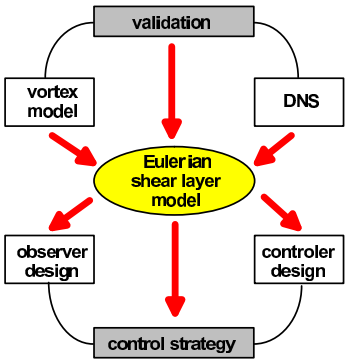

Figure 12: *Controller design based on Eulerian vortex models*

V Conclusions and outlook

A hierarchy of vortex models is presented for the two-dimensional coherent structures of the transitional flow around a backward-facing step. This flow is actuated by a local acoustic actuator at the upper edge. Experiments and simulations show that the local actuation leads to an earlier roll-up of the shear-layer vortices and to a reduction of the recirculation length.[3] This reduction of the dead-water zone is most pronounced at a Strouhal frequency around 0.4 and is smaller at other frequencies and comparable actuation amplitudes.

These coherent-structure dynamics are described by a hierarchy of Lagrangian vortex models where the resolution and the dimension are closely linked. The 'least-order' model of this hierarchy consists of a single point vortex which mimics the roll-up of the shear-layer in a vortex and its shedding. An even simpler representation of the recirculation zone has been employed in a separate, conceptual actuation study with control theory and dynamics systems analyses by the authors.[18]

A higher-order variant of this hierarchy is a vortex-blob model which describes well the formation of Kelvin-Helmholtz vortices and the dynamics of the recirculation zone with a few hundred vortices. This vortex-blob model also reproduces the reduction of the dead-water zone with the actuation and the dependency of the coherent structures on the actuation frequency. The length of the recirculation zone under natural and actuated conditions, the natural flow frequency, and the optimal actua-

tion frequency are predicted with reasonable quantitative accuracy. These modeling efforts indicate that the vorticity dynamics can be considered as an essentially inviscid process. The viscous and turbulent effects can be described with few physically motivated assumptions.

A non-hybrid 'Eulerian' vortex model with a constant number of vortices is proposed as an alternative to the Lagrangian variants. These models have comparable predictive capability at similar computational costs, but the mathematical form is better suited for the application of control-theory methods, in particular, for observer and controller design. The incorporation of control theory in the Eulerian and Lagrangian models and generalizations for other configurations are subject of active research at our Collaborative Research Center (Sfb 557).

Acknowledgment

The authors acknowledge funding and excellent working conditions of the Collaborative Research Center (Sfb) 557 "Control of complex turbulent shear flows" supported by the Deutsche Forschungsgemeinschaft (DFG) and hosted at the Technical University Berlin. B.R. Noack and G. Tadmor acknowledge funding of the DFG under grant NO 258/1-1 and of the U.S. National Science Foundation (NSF) under grants ECS 0136404, CCR 0208791, respectively. Valuable discussions with Andrzej Banaszuk (UTRC), Luca Cortelezzi (McGill Univ.), Ahmed Ghoniem (MIT), George Haller (MIT), Eckart Meiburg (UCSB), Igor Mezić (UCSB), and Mario Soteriou (UTRC) are acknowledged. Discussions and contributions of our team and our colleagues at the TUB, namely Ralf Becker, Werner Jürgens, Maiko Garwon, Carsten Gutknecht, and Michael Schlegel are appreciated. The three-dimensional flow visualization has been prepared with Tino Weinkauf using Amira 2.3 (http://amira.zib.de). The numerical data have been provided by H.-J. Kaltenbach and Maiko Garwon.

References

1. A.F. Ghoniem and Y. Gagnon, "Vortex simulation of laminar recirculating flow," J. Comput. Phys., vol. 68, pp. 346–377, 1987.

2. D. Wee, S. Park, R. Miake-Lye, A.M. Annaswamy, and A.F. Ghoniem, "Reduced-order modeling of reacting shear layer," AIAA Paper 2002-0478, 40th Aerospace Sciences Meeting and Exhibit, 2002.

3. A. Huppertz, Aktive Beeinflussung der Strömung stromab einer rückwärtsgewandten Stufe (transl.: active control of a flow downstream of a backward-facing step), PhD thesis, Fachbereich 10 'Verkehrswesen und Angewandte Mechanik,' Technische Universität Berlin, 2001.

4. C.M. Coats, "Coherent structures in combustion," Prog. Energy Combust. Sci, vol. 22, pp. 427–509, 1997.

5. B.R. Noack, I. Mezic and A. Banaszuk, "Controlling vortex motion and chaotic advection," Paper INV 4902, 39th IEEE Conference on Decision and Control 2000, pp. 1716–1723, 2000.

6. T. Weinkauf, H.-C. Hege, B.R. Noack, M. Schlegel, and A. Dillmann. "Coherent structures in a transitional flow around a backward-facing step," to appear in Phys. Fluids, vol. 15, 2003.

7. R. Becker, M. Garwon, C. Gutknecht, G. Bärwolff, and R. King, "Regelung aerodynamischer Strömungen am Beispiel einer rückwärtsgewandten Stufe (transl.: control of aerodynamics flows examplified for the backward-facing step)," Automatisierungstechnik, vol. 50, pp. 79–86, 2002.

8. H.-J. Kaltenbach and G. Janke, "Direct numerical simulation of flow separation behind a swept rearward-facing step at $Re_h = 3000$," Phys. Fluids, vol. 12, pp. 2320–2337, 2000.

9. M. Schlegel, B.R. Noack, and A. Dillmann, "Low-dimensional Galerkin models of transitional shear flows," In 55th Annual Meeting of the Division of Fluid Mechanics, American Physical Society, 2002.

10. W.T. Ashurst and E. Meiburg, "Three-dimensional shear layers via vortex dynamics," J. Fluid Mech., vol. 189, pp. 87–116, 1988.

11. B.D. Coller, B.R. Noack, S. Narayanan, A. Banaszuk, and A.I. Khibnik, "Reduced-basis model for active separation control in a planar diffuser flow," AIAA Paper 2000–2563, AIAA Fluids 2000 Conference and Exhibit, 2000.

12. J.P. Giesing, "Vorticity and Kutta condition for unsteady multi-energy flows," Trans. A.S.M.E., J. Appl. Mech., vol. 36, pp. 608–613, 1969.

13. G.H. Cottet and P. Koumoutsakos, Vortex Methods — Theory and Practice, Cambridge University Press, Cambridge, 2000.

14. L. Cortelezzi, "Nonlinear feedback control of the wake past a plate with a suction point on the downstream wall," J. Fluid Mech., vol. 327, pp. 303–324, 1996.

15. C.A.J. Fletcher, Computational Techniques for Fluid Dynamics; Volume II: Specific Techniques for Different Flow Categories, Springer, Berlin, 1988.

16. S. Narayanan, B.R. Noack, and E. Meiburg, "Reduced-order dynamical modeling of sound generation from a jet," AIAA Paper 2002-0073, 40th Aerospace Sciences Meeting and Exhibit, 2002.

17. E. Meiburg, "Three-dimensional vortex dynamics simulation," pp. 651–685, Kluver Academic Publishers, Dordrecht, 1995.

18. B.R. Noack, I. Mezic, G. Tadmor, and A. Banaszuk, "Optimal mixing in recirculation zones," manuscript submitted to Phys. Fluids, 2003.